Advanced Sonar with Velocity Compensation

Lindsay Kleeman

Intelligent Robotics Research Centre
Department of Electrical and Computer Systems Engineering
Monash University, Melbourne, Australia,
lindsay.kleeman@eng.monash.edu.au

Abstract

Robotics research is dependent on intelligent, fast, accurate, reliable and cheap sensors. Sonar sensing can fulfil these requirements. Moreover sonar physics provides robotics researchers with a natural selection capability for landmark detection in navigation problems. This paper presents a new sonar system that produces accurate measurement and on-the-fly single cycle classification of planes, corners and edges. The paper shows how double pulse coding of the transmitted pulse can be exploited to simultaneously reject interference and perform classification. On a moving platform, the velocity of the sonar sensor affects range and bearing measurements and is dependent on the target type. These effects are analysed in the paper. Effects of rotation are also considered. The analytical results derived in the paper for velocity generated deviations in sonar range and bearing estimates are compared with experimental data. The experiments show that the deviations are evident at speeds encountered in mobile robot research. Compensation of these effects can be achieved using the analytical expressions derived in the paper, the sonar information of range, bearing and target classification, and odometry measurements.

1. Introduction

Sonar sensing is common-place in robot applications, however *advanced* sonar sensing is not widely applied. What is meant by advanced sonar? This can be addressed by examining firstly sonar that is *not* advanced, such as the Polaroid Ranging Module (PRM) [17]. In its commonly applied form, PRM supplies a range estimate derived from thresholding the first echo[1] out to a maximum range of 10 meters. The beamwidth depends on range and target reflectivity. The user learns little about the target, the angle to the target, the strength of the echo or whether the echo comes from this sonar system or another. *Advanced* sonar can accurately determine angle, target classification, target strength to multiple targets and whether that sonar system owns an echo, allowing rejection of interference.

Accurate range and bearing measurements of multiple targets have been achieved in [6,10,11,12,15,16,19,23], interference rejection reported in [1,8,10,11,21], and target classification in [2,3,4,5,6,9,12,13,14,15,16,19,23].

Knowing the shape, or class, of a target assists in robot localisation and mapping applications. It enables prediction of how the target will appear from different sensor positions, and simplifies associating environmental features to a map. Mistakes in association can lead to persistent gross errors. This paper also shows that target classification is required to compensate for motion effects on range and bearing estimates.

Properties of acoustic wave propagation and the structure of indoor environments has lead sonar researchers to the adoption of three classes of target: *plane*, 90° concave *corner* and convex *edge*. The work in [12] provides a proof that the minimum requirements to classify targets into these categories are two transmitter positions and two receivers positions. The transmitter positions need not be distinct from the receiver positions.

Sonar relies on insonifying the environment in a *cyclic* fashion, so the energy emitted in one cycle has dissipated before a new cycle is commenced. In pulse-echo sonar this means a new pulse is not transmitted before there is a possibility that a previous pulse can be detected by a receiver. Similarly in CTFM [19] (continuous time frequency modulated) sonar a new frequency sweep is not commenced until the start of the previous acoustic sweep has died out.

[1] The gain increases in discrete steps with time in the PRM pre-amplifier and integration occurs before thresholding.

Prior to work described in this paper, sonar target classification for corners, planes and edges required multiple cycles to obtain coordinates of virtual images of a transmitter in two different positions [2,3,5,12]. Those methods require moving a single transmitter, or incorporating at least two sequentially fired transmitters into the sensor. Either way, in the interval between the two cycles there can be significant air or sensor movement that contributes to errors in the measurement, and the reduction of classification reliability. If the interval of time between transmitter firings can be reduced, reliability should be improved. Additionally, the latency before the target can be classified will be reduced.

This paper discusses an approach [9] that reduces this classification latency whilst still classifying targets as *corners, planes, edges*, or unknown. The classification is compressed into a single processing cycle by firing two transmitters almost simultaneously. Indeed, the precise separation serves to identify the sensor, providing interference rejection using *double pulse coding* – a technique presented for interference rejection alone in [11]. This paper shows that there is a natural synergy between classification and interference rejection. Moreover the signal processing is implemented on a DSP and can be performed at cycle rates (eg 30 Hz to 5 meters), allowing on-the-fly sonar classification and interference rejection.

Two objectives are pursued in this paper. The first is to present the capabilities of the advanced sonar system and provide an informed basis for comparison of advanced sonar with other sensing modalities. The second is to present new work aimed at understanding the effects of deploying this rapid sonar sensing approach on *moving* platforms. These results can then be used to fully exploit the advantages of rapid sensing techniques with known results. In particular, the effects of sensor velocities on range and bearing measurements are derived and verified experimentally. The experiments also confirm that velocity effects are indeed evident in measurements from an advanced sonar sensor.

This paper is organised as follows: Section 2 discusses how a DSP sonar sensor can be implemented to achieve an advanced sonar design. Techniques for extracting accurate range and bearing measurements are described in section 3, while section 4 illustrates how advanced sonar can naturally extract sparse landmarks – a useful property of sonar when combined with other sensors, such as vision and laser systems. Section 5 addresses the problem of interference rejection and presents results of experimental verification of difference approaches. On-the-fly classification approaches are outlined in section 6. The effects of a moving platform on range and bearing estimation are analysed in section 7. Section 8 presents experimental results that support the analytical results from section 7. Conclusions and future research ideas are then offered.

2. Sensor Design

In this section, the design of a DSP based sonar sensor is discussed. The sonar sensor is built from commercially available 7000 series Polaroid transducers [18] with their front grilles removed – this significantly reduces pulse lengths since the grille causes reverberation within the transducer. The sensor includes custom designed digital and analogue electronics, and a digital signal processor (DSP). The signal processing is implemented within the sensor and results relayed to a host computer via high speed serial communication. The sensor measures 150 by 100 by 70 mm and is powered by a singe 5 Volt supply. Results on range and bearing accuracy, once the speed of sound is calibrated, are reported in [12] and vary with air conditions. Typical office conditions give range error standards deviations of 0.2 mm and bearing error standard deviations of 0.1 degrees at 3 meters range. The sensor is capable of detecting walls to 8 meters, but echo sampling is stopped at 5 meters to increase speed.

2.1 Transducer Arrangement

The transducers are arranged in a square shown in Figure 1, where adjacent transducers are just 40 mm apart. An important feature of sonar is that time of flight errors are well correlated in time and space [12,11,20]. By placing two receivers close together, very accurate measurement of bearing can be achieved despite the short baseline [12], because the bearing calculation depends critically on the difference between the two times-of-flight from a single transmitter to the two receivers. The error in this difference is typically much smaller than the straight time of flight errors since these are highly correlated.

Additionally placing the two transmitters close together produces highly correlated errors for all the four time-of-flight measurements of a target – that is T1 to R1, R2 and T2 to R1, R2. This is important because the dominant factor in determining the class of a target is the difference between the two measured bearings [9]. Classification of targets with closely spaced transmitters has been achieved out to 5 meters [9].

The beam angle that the sensor can detect targets on both receivers depends on the target reflectivity and the range and is approximately 15 degrees off axis at 3 meters range for a perfect reflector such as a smooth plane.

In summary the receiver and transmitter close spacing exploits the spatial correlation of errors in time of flights to achieve accurate bearing estimation and reliable classification.

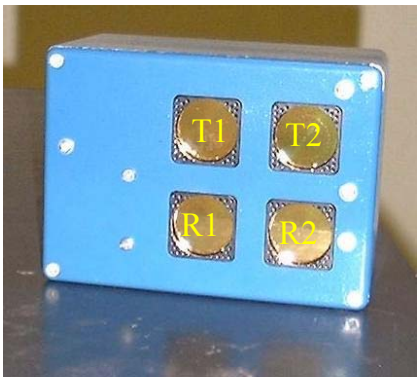

Figure 1 *- The DSP sonar sensor showing transmitters T1 and T2 and receivers R1 and R2.*

2.2 Electronics and Processing Hardware

Referring to Figure 2, the received signals are amplified, low pass filtered and digitised with 12 bit precision at a 1 MHz sample rate and processed on an Analog Devices 33 MHz ADSP2181. The DSP also generates the transmit waveforms and communicates with the host via an external buffered UART.

A pulse is fired from the right transmitter first, and rapidly followed from the left (200 μs delay is typical). Echoes are processed on the DSP, yielding up to four arrival times for reflections from each target.

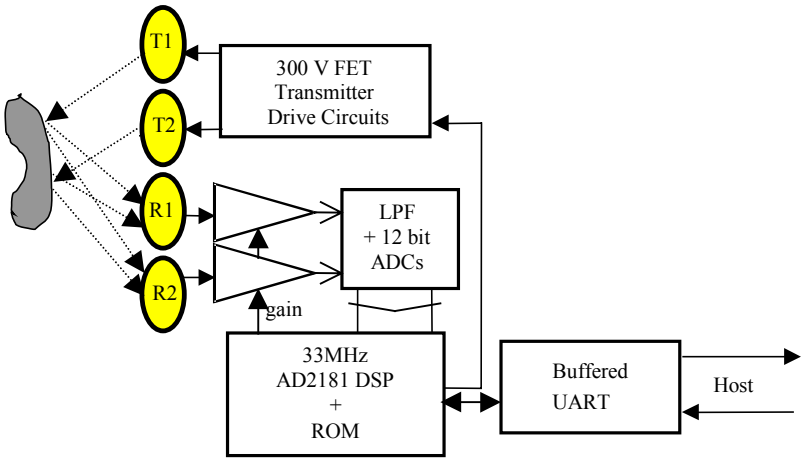

Figure 2 *- DSP sonar hardware block diagram.*

2.3 Interface

The sensor communicates with a host computer via a set of commands. These commands enable access to all levels of signal data within the sonar sensor, from the received pulse data samples up to the target range, bearing and classification. Low level access is implemented by the DSP sending to the host, sonar data structure addresses within the DSP memory space, so the host can interrogate intermediate results. In normal operation, the sensor fires repeatedly and packets of target information are send up the serial line to the host after processing of the echoes from the current cycle.

2.4 Time stamping and synchronisation

In real time sensing applications sensor measurements are of little value without time stamping. This is for two reasons – the sensor may be moving and measurements need to be fused with other sensors, and the targets may be moving. Facilities on the sonar sensor are provided for synchronising the sonar local time to the host time and providing a time stamp with every measurement set. Sonar time is maintained by a DSP timer that generates an interrupt every millisecond. Since the host time and sonar time will inevitably drift, synchronisation with the host is repeated every 2 minutes to ensure at most 2 milliseconds discepancy exists.

3. Range and Bearing Measurements

The aim of the sonar data processing is to extract the arrival times from echoes. The arrival times enable target range and bearing to be estimated using the speed of sound and receiver geometry. Arrival times are estimated using a technique known as matched filtering first used in RADAR systems [22]. Matched filtering obtains the arrival time by cross correlating the received echo with an echo template stored in the sensor. A template is a noise free pulse shape computed offline. The template shape depends on the angle of arrival to the transducer as shown in Figure 3. This dependency on angle can be accurately modelled by using convolution with the impulse response of a circular transducer [12]. The template is shifted across the echo to find the maximum correlation. By fitting a parabola to the maximum three correlations and their shift times, a very accurate arrival time estimate is obtained [12].

The software to process the sonar echoes has been optimised for speed. Careful design of the sonar front end electronics has led to the high signal to noise ratio and consequently the data processing is significantly simplified. In particular, matched filtering is performed only on sections of the echo signal deemed to be "pulses" by virtue of exceeding a threshold. The threshold is set to 7 noise standard deviations to avoid spurious triggering. Other sonar systems reported in the literature [16,10] perform expensive matched filtering on the entire received waveform since pulses cannot be separated reliably from noise as can be done in this system. A pulse commences 30 samples before exceeding the noise threshold and ends 30 samples after falling below the threshold, where the signal is sampled every microsecond. The number of samples per cycle is 17 and an echo lasts for about 80 microseconds. A further process of "pulse splitting" is applied to separate nearly overlapping pulses by searching for a local maximum within a 60 sample sliding window – further details are in [7]. Pulses as close together as 60 microseconds can be split and this results in the sensor being able to resolve targets separated in range by at least 10 mm.

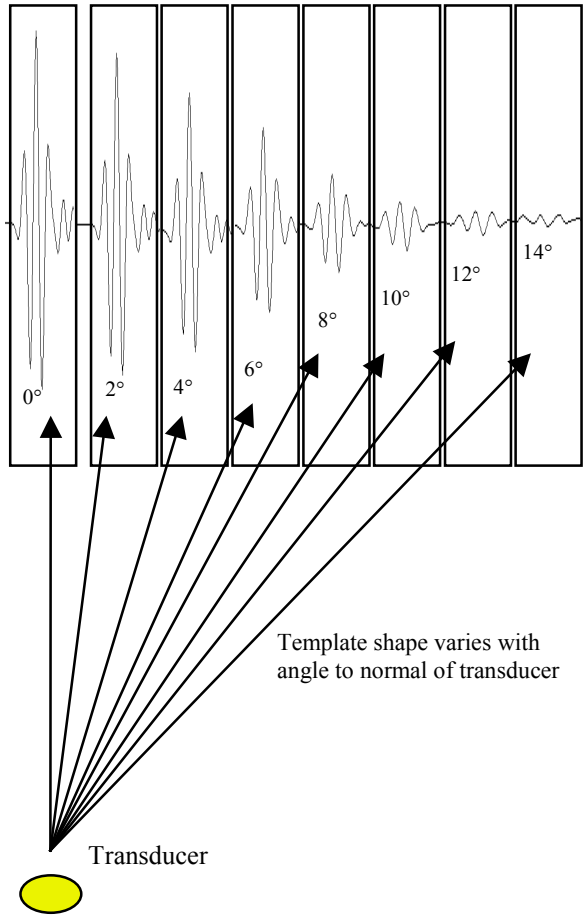

Figure 3 *– Template pulse shapes as a function of angle.*

The DSP software is organised into two stages. During the first stage, highly optimised assembly code performs on-the-fly processing of the samples from the two receivers to extract discrete pulses that exceed the noise floor. The second stage processes the extracted pulses with C code to partition closely spaced yet separable pulses and to extract arrival times using matched filtering. The processing steps are shown on an example echo signal in Figure 4.

Stage one has a main program and a timer interrupt routine that runs every microsecond. The timer interrupt service routine fetches the next two 12 bit ADC samples from the two receiver channels and places them into a circular buffer. The interrupt routine is also responsible for generating transmitted pulses and receiver gain changes.

The main program runs in a loop where each iteration processes the block of data acquired since the previous iteration. The two channels are processed independently through four stages: DC bias removal, thresholding, aggregation and storing into a pulse data structure

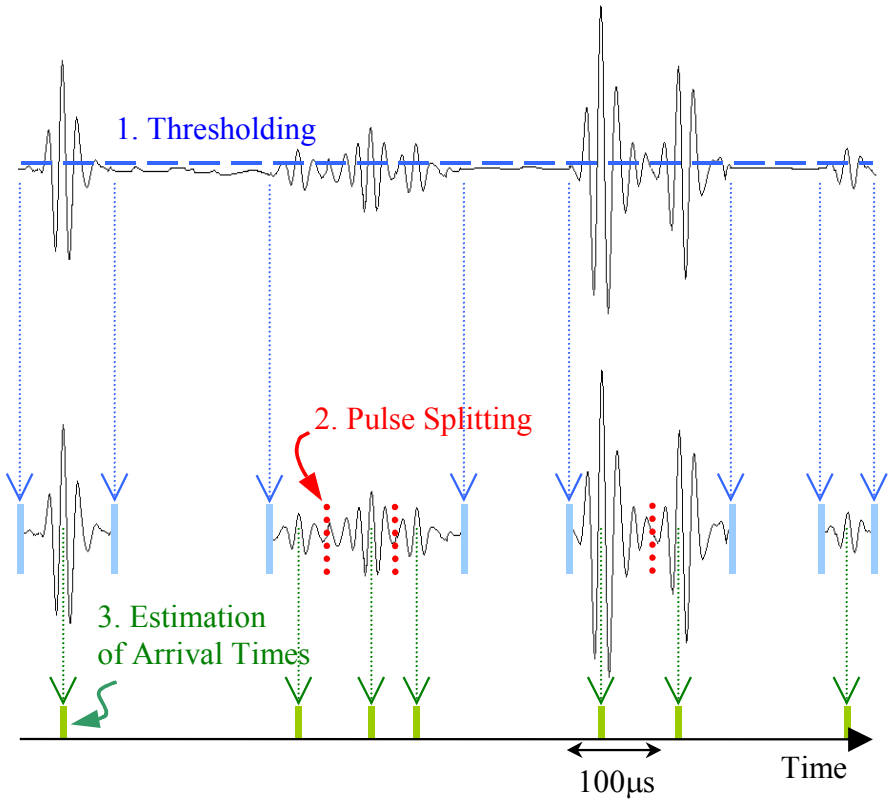

Figure 4 *– DSP processing steps to extract arrival times.*

3.1 Association

In order to derive the bearing angle to physical targets, pulse arrival times must be associated between the left and right receiver channels. Ambiguities are possible in this process when there are many closely spaced pulses. To guard against this, a conservative approach is adopted and possible ambiguities actively sought out and discarded. The effect of an incorrect association between two pulses is that the bearing angle is grossly in error.

Every pulse extracted from the left channel is compared with every pulse from the right. An association is declared reliable if the following conditions are met:

- Arrival times are consistent with the receiver physical spacing, *SEP* = 40 mm – that is arrival times differ by less than *sin(max_angle) * SEP / speed_sound*, which is approximately 60 microseconds for a *max_angle* of 30 degrees.
- Pulse amplitude ratio is between 0.5 and 2.0.
- Both left and right template to echo correlation coefficients are over 0.95

If only the last condition is not met, the association is flagged as 'unreliable'. Range and bearing of all associations are calculated [12] and called targets. If any pulse is associated with more than one pulse on the other receiver, all associations involving these pulses are demoted to 'unreliable'. Pulses that are not associated with any pulse on the other receiver are retained and are assumed to correspond to targets in the pointing direction of the receiver and are marked 'extremely unreliable'[2]. These targets, when combined with amplitude information from other measurements in different directions, can give an indication of the roughness and position of a surface [4].

[2] Essentially the same information that the Polaroid Ranging Module provides except echo amplitude is accurately known.

4. Natural Selection of Landmarks

In Figure 5, the sonar sensor is mounted on a mobile robot with panning mechanism and sent down a corridor. Whilst moving, the sonar performs "windscreen wiper" scans of the environment. Combining robot odometry and the sensor pan angle with sonar range and bearing measurements yields the map shown in Figure 5. The radius of the circle representing a target is proportional the echo amplitude measured by the sonar and indicates a measure of reliability of the target. There are several noteworthy characteristics:

- Features are sparsely distributed, reducing map complexity and increasing reliability of measurement to map association during robot localisation.
- Useful distinctive natural landmarks are common, such as the orientation and position of walls, positions of corners, edges or doorways.
- Reliable targets can be identified by sonar echo amplitude and pulse shape to template correlation coefficient.

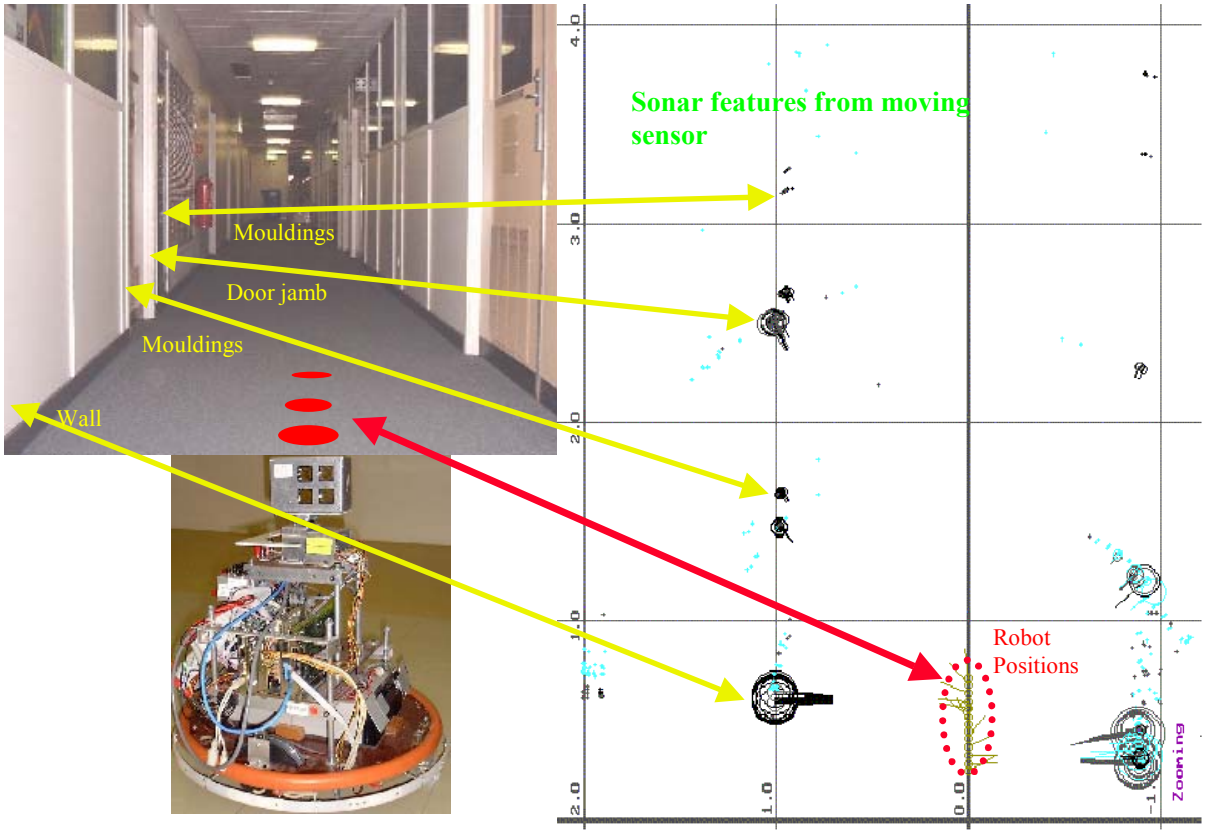

Figure 5 – *Examples of natural landmark extraction with advanced sonar.*

5. Interference Rejection

Interference rejection is dependent on recognising echoes that were transmitted from the same sonar sensor. Some form of encoding of the transmitted pulse can be deployed to this end. In this work the simplest compatible approach is taken and this is to transmit two identical pulses and use the *time separation* as the encoding information. Received pulses are examined and checked for this same time separation, subject to predictable Doppler variations due to robot motion [11]. Other more sophisticated coding techniques exist but result in longer pulses and additional processing overhead [10,16,21]. The time separation employed is greater than 150 micro-

seconds to avoid pulse overlap problems on the one receiver. Note also from section 3.1 that due to the close spacing of the receivers (40 mm) the association of echoes between receivers requires that the time difference between two receivers for the one echo must be less than 60 microseconds. Thus there is no confusion in association of echoes between receivers introduced by double pulse coding since the double pulse separation is much greater than the largest possible time difference between receivers for the same echo.

Two approaches can be used to validate that pulse pairs are properly separated and the same shape:

1. Work in [11] validates echoes by checking that the maximum difference between pulse waveforms, taken sample by sample, must fall below a threshold to be validated. Doppler effects slightly change the separation of returns on a moving robot. This shift is predictable from robot speed measurement using odometry provided the targets are stationary. Variations are accommodated in [11] by shifting and testing again.
2. The approach in [9,8] uses a similar algorithm except correlation between pulses is used rather than difference. The first return defines a matched filter that measures the time delay to the second pulse. This provides a direct measurement of the Doppler[3] shift due to relative velocity between target and robot, and may be useful in some applications.

The double pulse coding approach has been tested using experiments that introduce deliberate interference. Figure 6 shows a robot with two sonar systems that fire simultaneously – the lower one is the interfering source and the upper one is used to construct a map of the wall.

Figure 7 shows results from double pulse coded interference with a difference spacing to the double pulse coding used in the map building sensor. Note that the wall floor corner is seen as a phantom target beyond the expected wall position and double reflections also add other phantom targets. Note the lack of spurious readings in the map. Compare Figure 7 with Figure 8 where the same spacing is used by the interference and the mapping sonar. The interference is clearly present in the results. Figure 9 shows the results when the double pulse spacing is varied from cycle to cycle randomly for both sensors. Most interference is rejected, but not all. The remaining interference is due to coinciding random spacings and also environmental faking effects where a single transmitted interference pulse generates two echoes with a spacing coinciding with the random spacing. Since the interference is not synchronised to the mapping sensor, these occurrences do not repeat at the same position cycle to cycle and can be rejected. The advantage of randomly spaced double pulse coding is that no *a priori* code negotiating needs to be established between sensors. This allows multiple sensors to operate in the same environment without any cooperation.

[3] Doppler shift also has a time compression effect on the pulse shape that is insignificant due to the short pulse duration employed and the low robot speeds relative to the speed of sound.

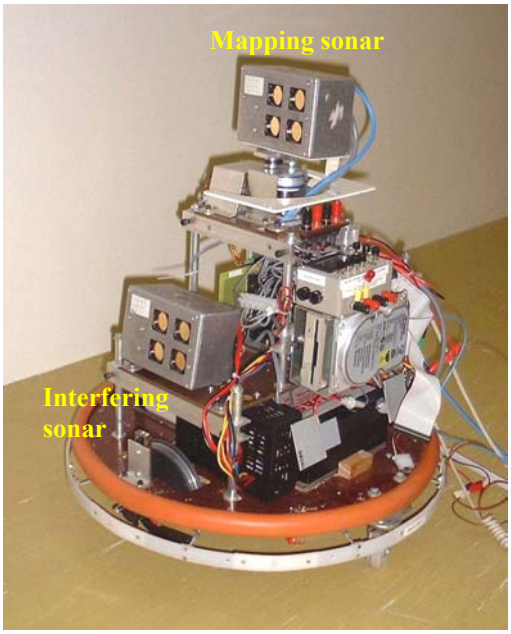

Figure 6 *– Interference experiments on a robot with two sensor firing at the same wall simultaneously.*

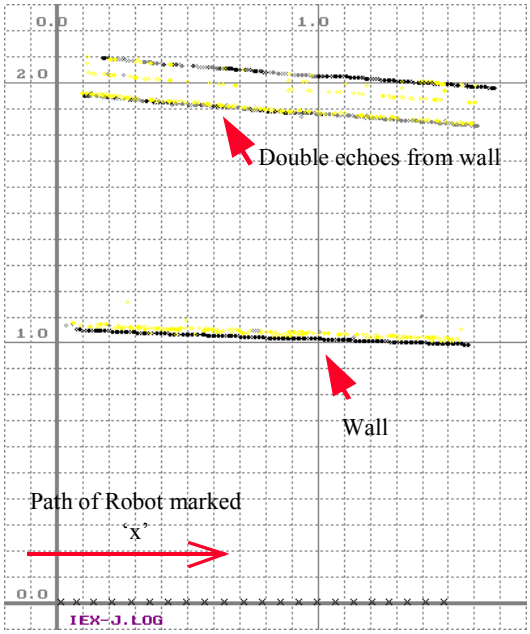

Figure 7 *– Interference from a double pulse source is rejected from another sonar using a different double pulse*

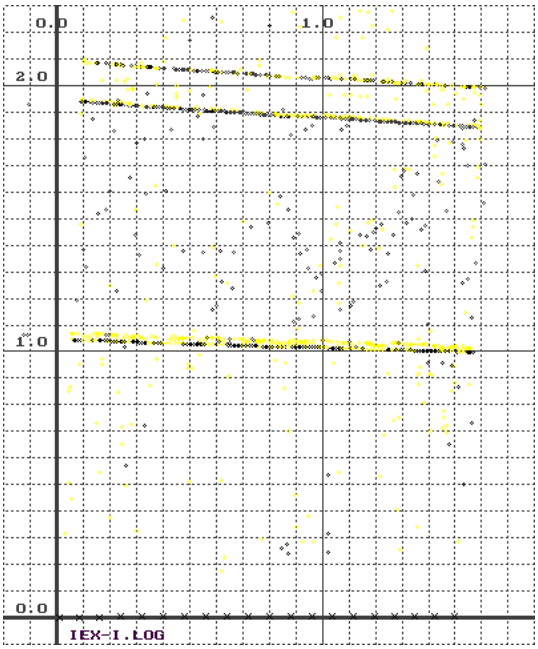

Figure 8 *– Interference is not rejected since both sensors use the same double pulse spacings.*

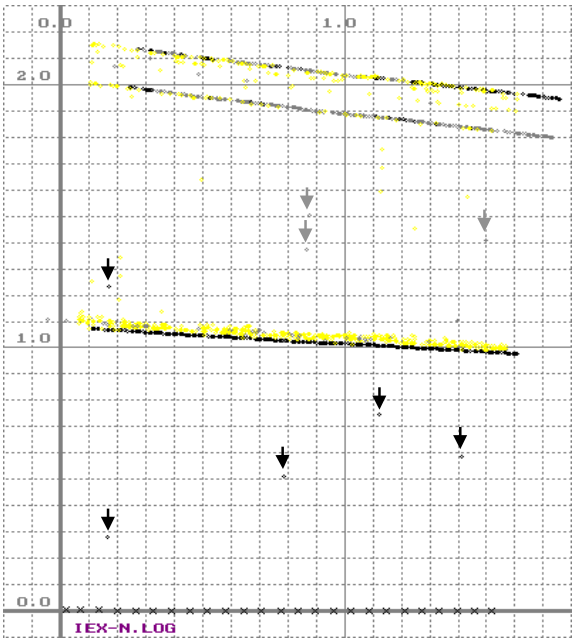

Figure 9 *– Random double pulse spacing interfering with random double pulse spacing – most but not all interference is rejected.*

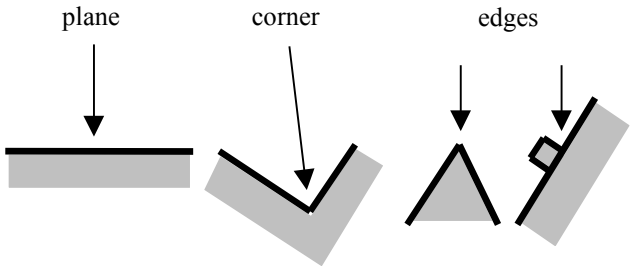

Figure 10 *– Target types that sonar can classify.*

6. Classification

Sonar target classification into planes, corners and edges, as shown in Figure 10, has been performed [12] in two sensor cycles by alternatively firing one transmitter and then the other. The basis for the classification can be explained simply by an analogy with virtual images and mirrors. Looking into a plane mirror, one's left eye appears on the left. Similarly with a sonar system the left transmitter (T2 in Figure 1) will be observed to the left of the right transmitter T1 using bearing measurement. However the situation is reversed when looking into a right-angled mirror – the left eye is observed on the right. Looking at a high curvature specular surface, such as a polished metal chair leg, the left and right eye images are compressed and appear to be at almost the same position – that is the angle between left and right images of the eyes is zero. Sonar classification can exploit the difference in bearing angles to the two transmitters to classify: positive difference indicates a plane, negative a corner and zero difference an edge. More sophisticated approaches have been published that exploit range in addition to bearing [12,9] using maximum likelihood estimation.

Recently, double pulse coding has been combined with classification to produce a classifying measurement in *one* sensing cycle [9]. Transmitter T2 is fired a known short time (eg 200 υsec) after T1 and echo arrival times are assembled from the two receivers. Given vertical planes, corners and edges, as commonly found in indoor environments, the distance of flight T1 to R2 is the same as T2 to R1. This property is exploited to determine the double pulse coding and hence transmitter identities (ie T1 or T2) of the received pulses. Therefore classification can be performed in one measurement cycle. Interference rejection, measurement and classification of targets has been implemented at 27 Hz using the DSP sonar system in Figure 1 [9].

7. Motion Compensation Analysis

In subsections 7.1 to 7.5 the effects of sensor linear velocity on the time-of-flight (TOF) and reception angle are analysed for the three cases of a plane, edge and corner target type. In subsection 7.6 rotation effects are discussed. The sensor is assumed to transmit from a point labelled T and receiver measurements are referred to the same position on the sensor labelled R, but due to the motion of the sensor R moves away from T, relative to a ground reference, over the duration of the time of flight.

For linear velocitythe distance between T and R is $TOF*v$, where v is the magnitude of the sensor velocity vector relative to the ground which is split into two orthogonal components v_x and v_y. The expressions derived for linear motion apply to any sonar sensor, since only the physics of sound propagation and reflection are used. All targets are assumed to be stationary.

7.1 Plane Analysis

The geometry of the plane target reflecting the transmitted pulse from T to R is shown in Figure 11. The TOF is broken up into two sections t_1 , representing the time to the plane and t_2, from the plane to the receiver R. The objectives of the analysis are to find the effect of the sensor velocity on the $TOF=t_1+t_2$ and the angle of reception, θ, with respect to a stationary observer. The effect on the reception angle of a moving observer is discussed in the next section.

Notice that from the right-angled triangle formed by T and the distance d_1 from the plane, that

$$\sin\theta = \frac{t_1 v_x}{t_1 c} = \frac{v_x}{c} \tag{1}$$

and

$$\cos\theta = \sqrt{1-\left(\frac{v_x}{c}\right)^2} \tag{2}$$

where c is the speed of sound. For small velocities relative to c:

$$\theta = \sin^{-1}\left(\frac{v_x}{c}\right) \cong \frac{v_x}{c} \tag{3}$$

From the same triangle

$$\cos\theta = \frac{d_1}{t_1 c} \Rightarrow t_1 = \frac{d_1}{c\cos\theta} \tag{4}$$

From the right-angled triangle involving the reflected path to R:

$$\cos\theta = \frac{(t_1+t_2)v_y + d_1}{t_2 c} \Rightarrow t_2 = \frac{(t_1+t_2)v_y + d}{c\cos\theta} \tag{5}$$

Adding equations (4) and (5) and solving for $TOF=t_1+t_2$ with help from equation (2)

$$TOF = \left(\frac{2d_1}{c}\right)\frac{1}{\sqrt{1-\left(\frac{v_x}{c}\right)^2}-\frac{v_y}{c}} \tag{6}$$

Note that the first factor in equation (6) represents the zero velocity solution for TOF and the second factor represents the effect of non-zero velocity and is close to unity for small velocities compared to the speed of sound.

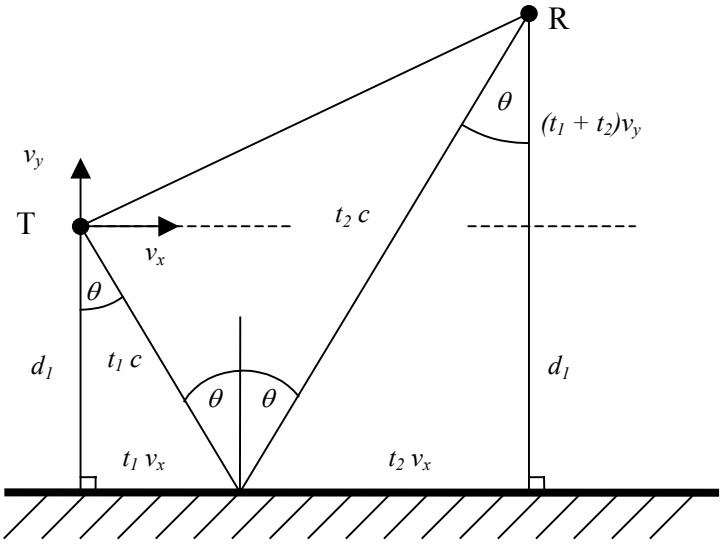

Figure 11: *Plane target with Sensor Movement*

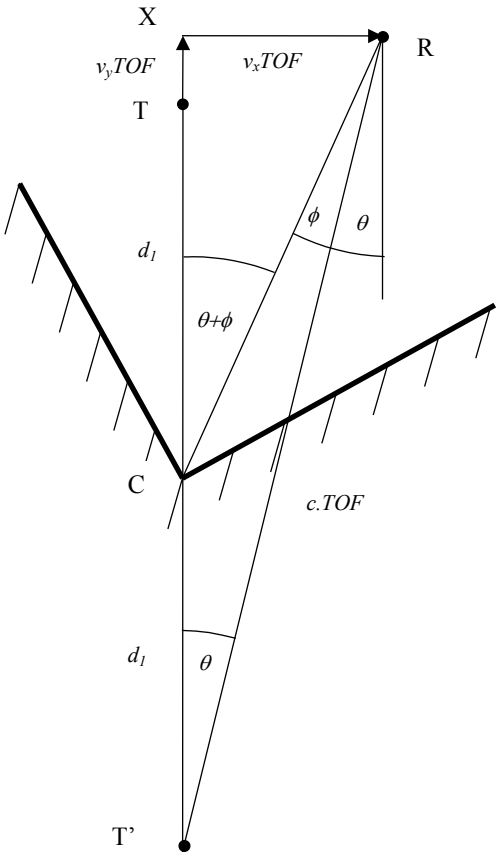

Figure 12: *Corner Geometry*

7.2 Corner Analysis

The geometry of the corner target reflecting the transmitted pulse from T to R is shown in Figure 12. The virtual image of T is shown as T' which is obtained by reflecting though both orthogonal planes of the corner, resulting in a reflection through the corner intersection point C.

Similar to the plane analysis, the objective is to find the motion altered TOF and reception angle discrepancy from the direction to the corner C, shown as ϕ in Figure 12. Starting with the right-angled triangle T'XR

$$c^2 TOF^2 = \left(2d_1 + v_y TOF\right)^2 + v_x{}^2 TOF^2 \tag{7}$$

Solving equation (7) for *TOF* yields:

$$TOF = \frac{2d_1}{c}\left[\frac{\sqrt{1-\left(\frac{v_x}{c}\right)^2}+\frac{v_y}{c}}{1-\left(\frac{v}{c}\right)^2}\right] \tag{8}$$

where $v^2=v_x^2+v_y^2$. Note that the first term of (8) represents the zero velocity solution for the TOF and the second term represents the effect of velocity and is close to unity for small velocities compared to the *c*.

The angle ϕ in Figure 12 represents the ground referenced angle deviation caused by the motion of the sonar sensor. This angle is now derived.

From the right-angled triangle T'XR

$$\tan\theta = \frac{v_x TOF}{2d_1 + v_y TOF} \tag{9}$$

and from triangle CXR

$$\tan(\theta+\phi) = \frac{v_x TOF}{d_1 + v_y TOF} \tag{10}$$

From equations (9) and (10)

$$\begin{aligned} &\frac{\sin(\theta+\phi)}{\cos(\theta+\phi)} = (2-k)\frac{\sin\theta}{\cos\theta} \\ &where\ \ k = \frac{v_y TOF}{d_1 + v_y TOF} \end{aligned} \tag{11}$$

expanding the *sin* and *cos* sums and rearranging gives

$$\tan\phi = \tan\theta\left(\frac{1-\sin^2\theta}{\frac{v_y TOF}{d_1}+1+\sin^2\theta}\right) = \left(\frac{v_x}{\frac{2d_1}{TOF}+v_y}\right)\left(\frac{1-\sin^2\theta}{\frac{v_y TOF}{d_1}+1+\sin^2\theta}\right) \tag{12}$$

For v_x, $v_y << c$, $\sin\theta << 1$ and $\frac{2d_1}{TOF} \cong c$ and so equation (12) leads to the approximation

$$\phi \cong \frac{v_x}{c} \tag{13}$$

7.3 EdgeAnalysis

An edge re-radiates the transmitted ultrasound from a point source, and therefore the reception angle with respect to a stationary observer is unaffected by motion as shown in Figure 13. The TOF however is changed due to the new receiving position.

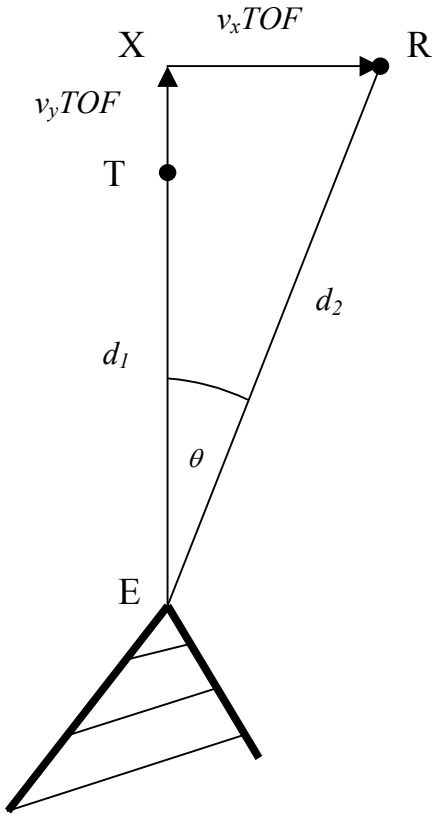

Figure 13: *Edge Geometry*

From the right-angled triangle XER

$$d_2{}^2 = \left(d_1 + v_y\right)^2 + v_x{}^2 TOF^2 \tag{14}$$

and also

$$d_1 + d_2 = c\,TOF \tag{15}$$

Solving equations (14) and (15) for the TOF yields

$$TOF = \frac{2d_1}{c}\left(\frac{1+\frac{v_y}{c}}{1-\frac{v^2}{c^2}}\right) \cong \frac{2d_1}{c}\left(1+\frac{v_y}{c}\right) \tag{16}$$

where the approximation in equation (16) is valid for $v<<c$.

7.4 Angle of Arrival Relative to the Moving Observer

The expressions for the reception angle in the previous section are based on an observer that is stationary with respect to the propagating medium, air. Suppose now the observer is moving at the same velocity as the sensor – which of course is the case in practice. Suppose a wave front arrives at an angle α relative to air, as shown in Figure 14. The velocity components of the wave front relative to the observer, w_x and w_y are as follows

$$\begin{aligned} w_x &= c\sin\alpha - v_x \\ w_y &= c\cos\alpha - v_y \end{aligned} \tag{17}$$

therefore, from equations (17) the observed angle of arrival, β is given by

$$\tan\beta = \frac{c\sin\alpha - v_x}{c\cos\alpha - v_y} = \frac{\sin\alpha - \frac{v_x}{c}}{\cos\alpha - \frac{v_y}{c}} \tag{18}$$

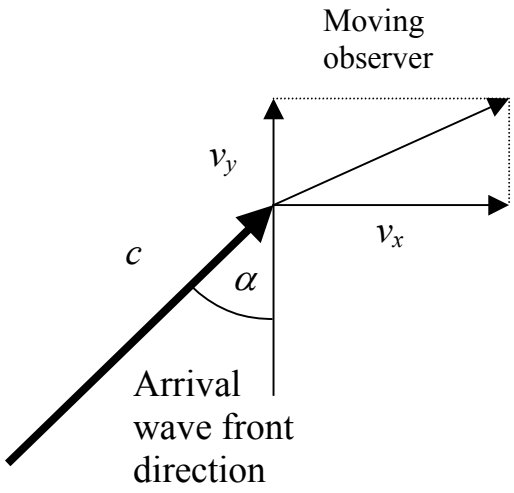

Figure 14: *Moving observation of a wave front*

7.5 Summary of Observed Approximate Arrival Angles

In this section, the previous results are approximated for speeds that can be expected on a mobile robot carrying the sonar sensor. The speed is assumed to be no more than a few meters per second – that is less than 1% of the speed of sound (typically 340 m/s at room temperature).

From equations (18) and (1), for a plane, the arrival angle relative to the sensor is exactly zero:

$$\beta_{PLANE} = \tan^{-1}\left(\frac{\frac{v_x}{c} - \frac{v_x}{c}}{\cos\alpha - \frac{v_y}{c}}\right) = 0 \tag{19}$$

This is no surprise when one realises that the wavefront follows a path relative to the moving sensor on a line seen to be perpendicular to the plane from the sensor's perspective. That is the wavefront forward velocity component is always the same as the sensor's due to reflection preserving this component.

The situation for a corner is quite different, since the angle ϕ results in a wavefront that appears to come forward (*ie* displaced in the same direction as the sensor motion) from the real corner direction, as can be seen in Figure 12. The effect of the moving observer doubles this effect as seen by equations (18) and (13)

$$\beta_{CORNER} \cong \tan^{-1}\left(\frac{-\frac{v_x}{c} - \frac{v_x}{c}}{\cos\alpha - \frac{v_y}{c}}\right) \cong -\frac{2v_x}{c} \tag{20}$$

For the edge there is just the moving observer effect:

$$\beta_{EDGE} \cong \tan^{-1}\left(\frac{0-\frac{v_x}{c}}{\cos\alpha-\frac{v_y}{c}}\right) \cong -\frac{v_x}{c} \tag{21}$$

7.6 Sensor Rotation Effects

This subsection briefly discusses the effects of rotation of the sensor. The echo arrival angle of the sensor is derived from the measurement of the time of flights from the two closely spaced receivers. This echo arrival angle is used as the bearing to the reflector and applies at the time of reception of the echo rather than the time of transmission, Rotation of the sensor can have two effects:

1 The effective beamwidth of the sensor can be reduced by the receiver rotating away from the target during the time of flight of the echo. There is also the possibility that the receiver will detect a target undetectable when stationary by rotating *towards* that target. If the receiver rotates more than half the beam width of the sensor away from the target during the time of flight of the echo, no echo will be detected. Assuming we have a half beamwidth of approximately 15 degrees and a 3 meter range, then the time of flight is approximately17.5 msec and therefore a rotation of at least 857 degrees per second is needed to exceed the half beam angle during the time of flight. For rotation speeds of less than 90 degrees per second employed on the robot described in the next section, this effect is not significant.

2 The measurement of the arrival angle may be slightly affected by a change in position of the second receiver during the time of flight between the first receiver and the second. Suppose the receivers are *SEP* distance apart, then for an echo arriving at an angle of θ to the normal of the receiver transducers, the time difference, t_{diff} for a stationary sensor is given by:

$$t_{diff} = \frac{SEP\sin\theta}{c} \tag{22}$$

If the sensor is rotating at ω radians per second about the R1 in Figure 1, then the actual measured time difference for a rotating sensor is:

$$t_{diff\_rot} = \frac{SEP\sin(\theta+\omega t_{diff\_rot})}{c} \cong \frac{SEP\sin(\theta+\omega t_{diff})}{c} \cong t_{diff}(1+\omega\frac{SEP\cos\theta}{c}) \tag{23}$$

where the first approximation applies for $\omega\, tdiff\_rot$ << angle error of the sensor which is of the order of 0.1 degrees. To give some numerical perspective to this, *tdiff* is less than 60 microseconds in practice and thus an angular speed of at least 1667 degrees per second would be required to generate an error of 0.1 degrees! The second approximation in equations (23) is obtained from a first order Taylor expansion about θ. The effect on the measured time difference between the two receivers is thus not significant for the rotational speeds encountered by anticipated sensor deployments.

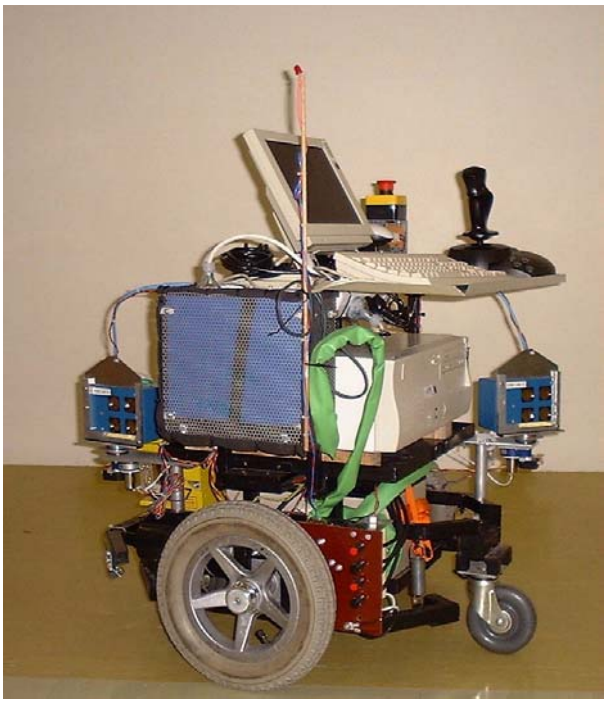

Figure 15 *Two DSP sonar sensors mounted panning mechanism on a mobile robot*

8 Experimental Results

The mobile robot shown in Figure 15 was programmed to follow straight line paths, accelerating up to 1 m/sec in approximately 0.5 m and travelling for approximately 3 m before stopping. The sonar systems are mounted on active PID controlled panning mechanisms with angle encoder resolution of 0.18 degrees (0.003 radians). The results of tracking a wall in the laboratory with the front sonar are shown in Figure 16, where the robot position was derived from wheel odometry measurements. These results illustrate the ability of the sensor to perform classification of planes whilst the robot is in motion. Note that this is not possible in sonar systems that fire two transmitters successive measurement cycles as much as 100 milliseconds apart as in [12] since significant robot motion uncertainty accumulates in this time making classification unreliable. The sonar system presented here achieves classification by firing both transmitters in rapid succession 200 microseconds apart – that is about 500 times faster.

The wall angle measured by the sonar was investigated at different speeds along the wall by the robot. The robot accelerates to full speed in less than 0.5 meters and travels for 1 meter at constant speed before slowing and stopping at 2 meters. The mean and standard deviations of the angle during motion and stationary at the end of travel are shown in Table 1, where wheel odometry measurements have been used to compensate for robot orientation changes during motion. The average angles in motion and stationary are very close, supporting the analysis result that no difference should be evident. The standard deviations in angles are consistently higher when in motion due to robot motion, small variations in the wall surface and changing air conditions.

Table 1 – Sonar Angle Statistics for Wall Following at Different Speeds

Robot Speed (metres/sec)	Mean angle (radians)		Standard deviation of angle (radians)	
	0.5 to 1.5 meters travel (constant speed)	End of travel (stationary)	0.5 to 1.5 meters travel (constant speed)	End of travel (stationary)
0.2	1.5159	1.5197	0.0025	0.0014
0.4	1.5297	1.5200	0.0031	0.0005
0.6	1.5302	1.5301	0.0027	0.0017
0.8	1.5254	1.5249	0.0037	0.0017
1.0	1.5219	1.5211	0.0031	0.0015

In another experiment, the robot moved at speeds up to 1 m/sec whilst the front sonar tracked and classified a corner as shown in Figure 18. The sonar classified the target as a corner on almost all measurements, despite being near the limit of its classification range of 5 meters. This experiment demonstrates the ability of the sonar sensor to perform on-the-fly classification of corners.

Figure 17 shows the deviation in angle as the robot moved. The data was generated by choosing a speed of sound so that the average reported position of the corner was the same at the start and finish of the 3 meter run where the robot was stationary. This point was then used as the ideal corner position and the deviation of angle is calculated as the difference between the sonar measured angle and the angle to the ideal corner. The deviations in angles are plotted in Figure 17 for different robot speeds.

The theoretical angle deviation expected from the sonar motion from equation (20) is shown on the plots as a dashed horizontal line - for example at 1.0 meters per second, this is 0.006 radians. In all plots, the robot starts at rest at a vertical distance x=0.3 and accelerates at 6.7 m/s/s to the maximum speed. The mean and standard deviation of the errors of the angle measurements are shown in Table 2 for both compensated and uncompensated data. The data is derived from the same data as represented in Figure 17 after 1 meter and before 3 meters travelled to ensure full robot speed is attained. The sources of errors are:

1. the robot rocking during motion due to rubber wheels and a spring loaded back castor wheel combined with backlash in the wheel gear boxes contributing to slightly uneven motion control.
2. the encoder measuring the pan angle of the sonar sensor. This has a resolution of 0.003 rad. that can result in errors of 0.0015 rad if no linearities errors are present.
3. sonar measurement errors which are of the order of ±0.002 rad and vary in a correlated fashion with a time constant of several seconds [11]. This correlation is evident in the time scaling of the errors at different speeds in Figure 17 – faster robot speeds result in less measurements per meter.
4. odometry errors which are comparatively small when travelling in a straight line. The odometry position and orientation estimates are updated every 10 msecs on the robot and interpolation is used to reference odometry estimates at the time of sonar echo arrival. Sonar and robot time base synchonisation is maintained to within an estimated 2 msecs at all times.

Note that the errors at x=3.2 in Figure 17 can be attributed to the robot lurching on its rubber inflated tyres as it stops abruptly.

Table 2 – Mean and Standard Deviations of Motion Compensated and Uncompensated Angle Errors Derived from 1 meter to 3 meter in the Travel of Figure 17.

Robot speed (m/sec)	Mean Angle errors (radians)		Standard Deviation Angle Errors (radians)	
	Velocity compensated	Not compensated	Velocity compensated	Not compensated
0.2	0.0004	0.0016	0.0025	0.0025
0.4	-0.0005	0.0018	0.0025	0.0025
0.6	-0.0003	0.0032	0.0024	0.0024
0.8	-0.0010	0.0037	0.0031	0.0031
1.0	-0.0013	0.0046	0.0029	0.0029

The effects of changes in range measurements to a plane as the robot moves towards the plane are shown in Figures 19 and 20. Initially the sonar is 5.1 meters from the plane and stationary. The range deviations are obtained from subtracting the y component of the plane position estimate obtained from sonar and robot odometry measurements from the true position of the plane. The true position is obtained by adjusting the speed of sound so that the start and end plane position estimates match. Figures 19 and 20 also show the predicted deviation based on equation (6) where the d_1 is obtained from the sonar range and odometry, v_x is zero and v_y is 0.6 m/s. The difference between the predicted and measured range deviations can be explained by the error sources 1, 3 and 4 listed above. The odometry to sonar synchronisation error of 2 msec would account for a maximum error of 1.2 mm. Note that the measurements shown in Figure 20 indicate the range errors of the sonar at start and finish of the motion are much smaller than 1 mm. The major component of error in this experiment is attributed to the robot rocking forwards and backwards – this is also evident just after the robot stops at samples 200 to 250 in Figure 20. This error may be significant in the context of map building and localisation under dynamic robot conditions.

A quantitative comparison is made between the uncompensated and compensated range measurements based on the means and standard deviations of the errors from the start of motion at sonar sample 70 to the end in Figure 20. The mean uncompensated error is 2.03 mm whilst the compensated error mean is –0.32 mm. Note the significant bias introduced by not compensating for the motion effects. The error standard deviations are 2.4 mm for uncompensated and 1.9 mm for compensated and are attributed to the robot rocking motion mentioned above.

The angle and range deviation results presented in this section support the theoretical models presented in Section 7 and indicate that the effects are measurable. Compensation can be achieved using equations (6, 8, 16, 20, 21), and measurements from sonar range, bearing and odometry speed together with sonar classification information.

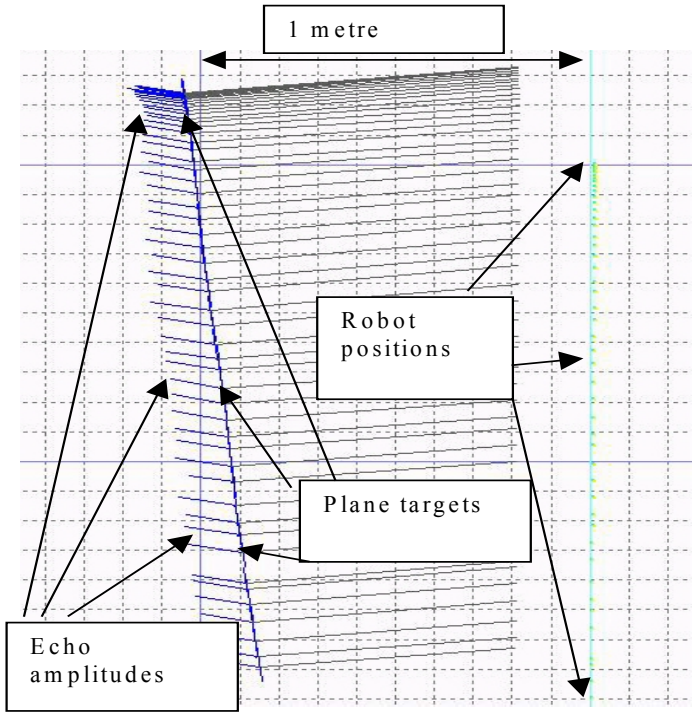

Figure 16: *Robot map from tracking and classifying a plane at a speed of 1 m/sec. The robot stops at the top.*

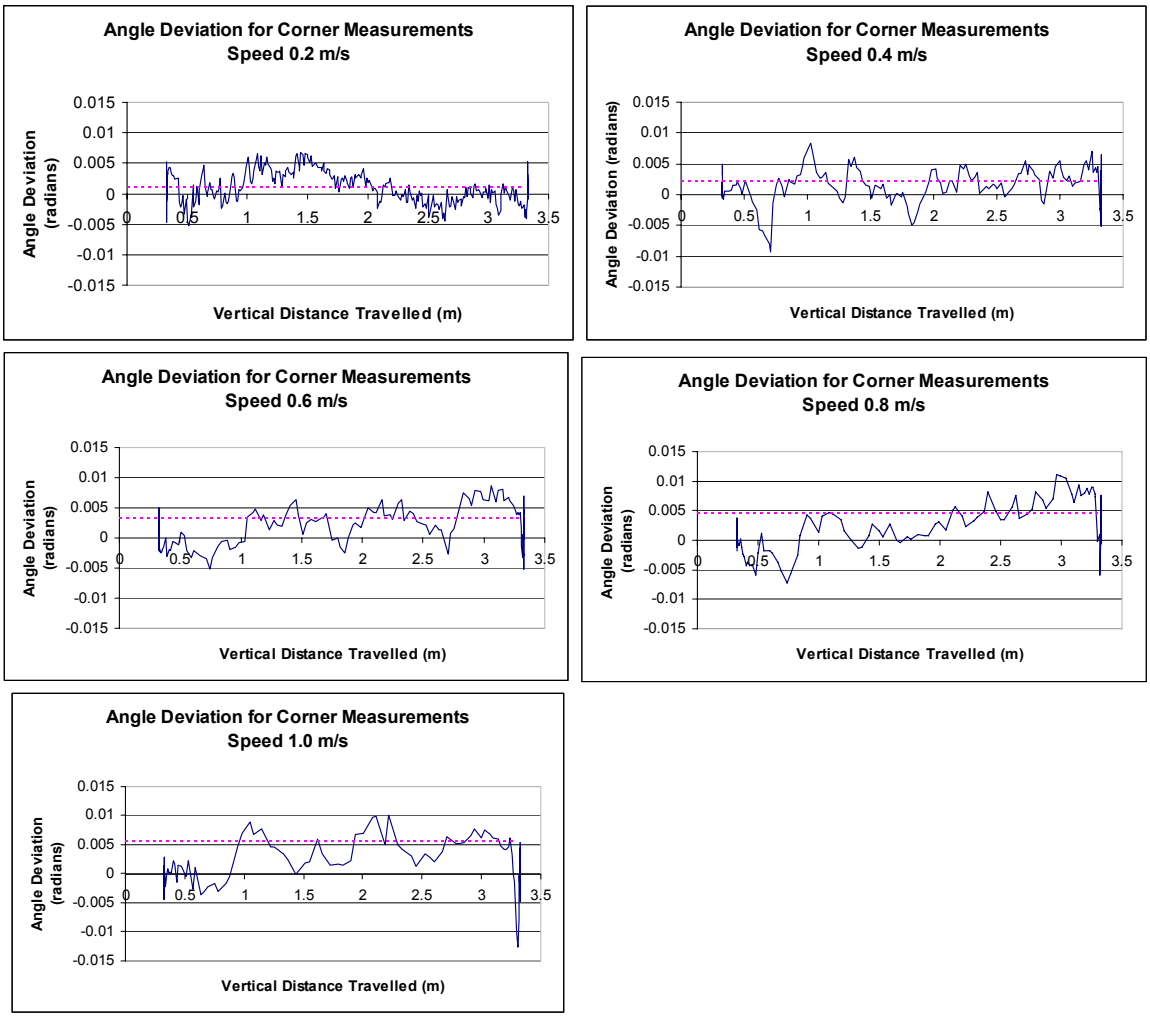

Figure 17: *Angle measurement error of the corner in Figure 18 with different robot speeds corner. The predicted shift in angle is shown as the dashed line. The start and ending angle errors have an average of 0 as the robot is stationary.*

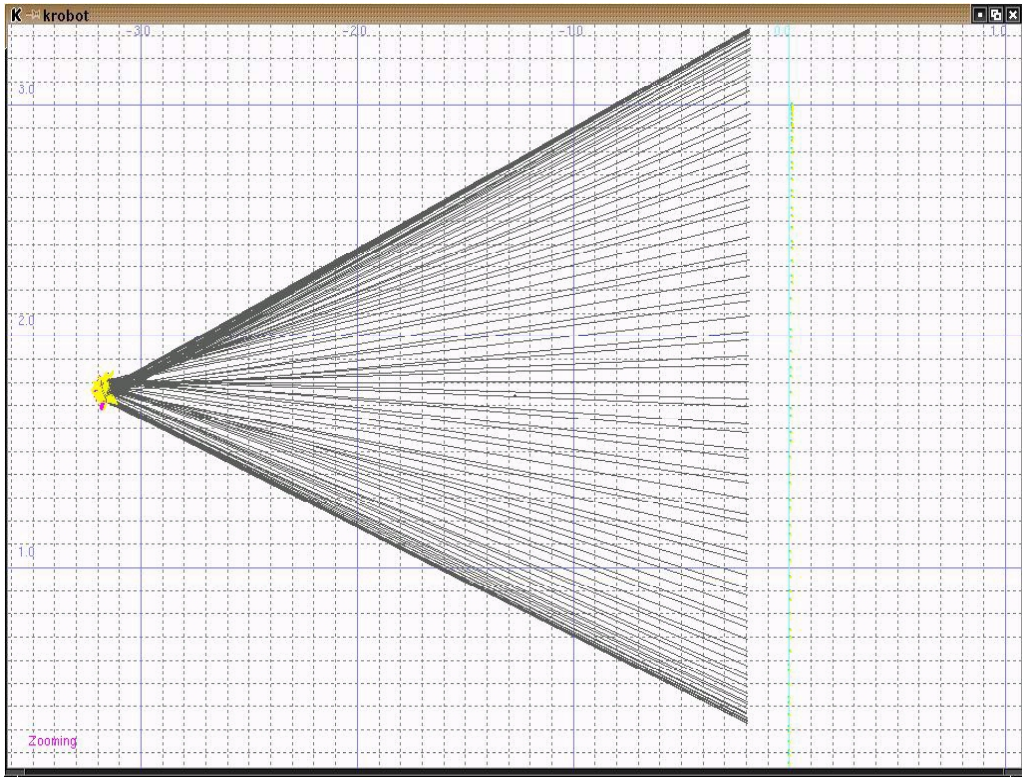

Figure 18: *Robot map from tracking and classifying a corner at 1 m/sec.*

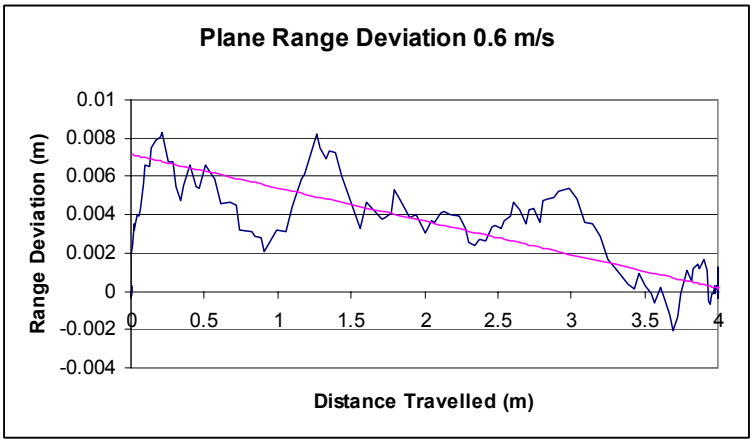

Figure 19: *Range deviation in measurements of a plane from the robot travelling towards the plane. The smooth line is the fitted model in equation (6) using the sonar range and a speed of 0.6 m/s. The plane is initially 5.1 meters from the sonar.*

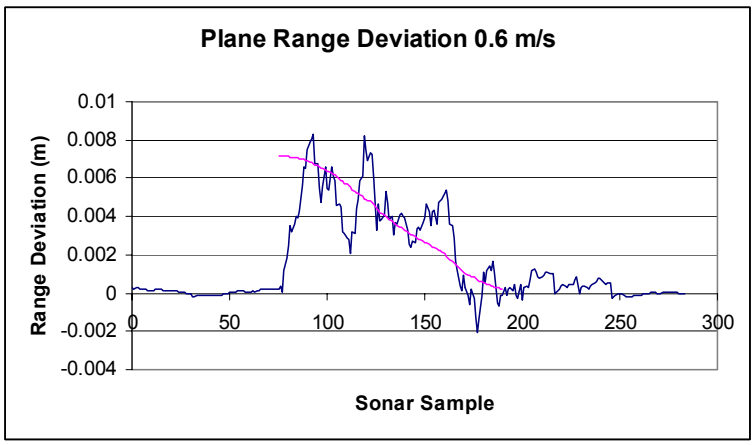

Figure 20: *The same experiment as in Figure 19, showing the range deviation against sonar sample. This illustrates the small errors in the sonar range at the start and end where the robot is stationary. Note that the robot is lurching after abruptly stopping at samples 200 to 250.*

9. Conclusions and Future Work

This paper has presented capabilities of an advanced sonar system implemented with a DSP, custom electronics and firmware. The term "advanced sonar" has been defined as sonar that delivers accurate range and bearing measurements with interference rejection and classification, all at high repetition rates. The paper has presented a new classification approach that operates in a single measurement cycle allowing a moving sensor to perform robust classification. Moreover the double pulse timing between two different transmitters has the added benefit of identifying the sonar source and thus allowing crosstalk and interference to be rejected, again in a single measurement cycle. The classification technique presented in the paper has been shown experimentally to work "on-the-fly" – that is when the sensor is moving at speeds of up to 0.6 meters per second. At speeds above 0.6 meters per second towards or away from a reflector, the double pulse separation changes enough to cause false interference rejection. This can be avoided simply by passing motion information to the sensor, so that pulse separation can be compensated.

The second half of the paper has presented a new analysis of the effects of motion on sonar range and bearing measurements. The analysis applies to any sonar system. The motion analysis has been experimentally tested and motion effects have been shown to be evident at speeds normally encountered by mobile robots. These results will be important when on-the-fly sonar map building is researched further.

An area of future research is error modelling of range and bearing estimates from stationary and moving sonar systems, extending work by Sabatini [20]. One promising avenue is using the difference in time of flights T1R2 and T2R1 as an air quality monitor and predictor for range and bearing error statistics that vary considerably with time. Optimal fusion of sonar with other sensor modalities would be one outcome of that research.

Acknowledgments

Funding is acknowledged from the Australian Research Council with the Discovery Project DP0210359 "Advanced Sonar Sensing for robotics". The design, construction and testing skills of Steven Armstrong are gratefully acknowledged. Andrew Heale's highly optimised contributions to the DSP sonar system have been invaluable.

References

[1] Borenstein J, Koren Y (1995) Error eliminating rapid ultrasonic firing for mobile robot obstacle avoidance. IEEE Trans. Robotics & Automation, Vol 11, No 1, pp 132-138.

[2] Barshan, B.; Ayrulu, B.; Utete, S.W (2000) "Neural network-based target differentiation using sonar for robotics applications" IEEE Transactions on Robotics and Automation, Vol 16 No 4 , pp. 435 -442

[3] Barshan, B and Kuc, R (1990), "Differentiating sonar reflections from corners and planes by employing and intelligent sensor", IEEE Trans. Pattern Anal. Machine Intell., Vol 12 No. 6, pp. 560-569.

[4] Bozma O, Kuc R (1991) "Characterizing pulses reflected from rough surfaces using ultrasound". Journal Acoust Soc of America, Vol 89, No 6, pp 2519-2531.

[5] Bozma O, Kuc R (1991) "Building a sonar map in a specular environment using a single mobile robot", IEEE Trans. Pattern Anal. Machine Intell., Vol 13, pp. 1260-1269.

[6] Chong KS, Kleeman L (1999) Feature-based mapping in real, large scale environments using an ultrasonic array. Intern Journal Robotics Research, Vol 18, No 1, pp 3-19.

[7] A. Heale and L. Kleeman, "A real time DSP sonar echo processor", IEEE/RSJ International Conference on Intelligent Robots and Systems, Takamatsu, Japan, October 2000, pp 1261-1266.

[8] Heale A, Kleeman L (2000) A sonar sensor with random double pulse coding. Australian Conf on Robotics & Automation, Melbourne, pp 81-86.

[9] Heale A, Kleeman L (2001) Fast target classification using sonar. IEEE/RSJ Intern. Conf on Intelligent Robots and Systems, Hawaii, USA, pp. 1446-1451.

[10] Jorg K, Berg M (1998) Mobile robot sonar sensing with pseudo-random codes. Proceedings IEEE Conf. on Robotics & Automation, Belgium, pp 2807-2812.

[11] Kleeman L (1999) Fast and accurate sonar trackers using double pulse coding. IEEE/RSJ Intern Conf on Intelligent Robots & Systems, Kyongju, Korea, pp 1185-1190.

[12] Kleeman L, Kuc R (1995) Mobile robot sonar for target localization and classification. International Journal of Robotics Research, Vol 14, No 4, pp 295-318.

[13] Kuc, R (2001). "Pseudo-amplitude scan sonar maps", IEEE Transactions on Robotics and Automation, Vol. 17 No. 5, pp. 767 –770.

[14] Kuc, R.; Kirichenko, M.F.; Lepekha, M.P. (1999), "Adaptive and mobile biomimetic sonar recognizes objects from echoes",OCEANS '99 MTS/IEEE. Riding the Crest into the 21st Century , Vol. 2, pp. 707 –712.

[15] Kuc, R. (1997), "Biomimetic sonar locates and recognizes objects ", IEEE Journal of Oceanic Engineering, Vol. 22 No. 4, pp. 616–624.

[16] Peremans H, Audenaert K, . Campenhout JMV (1993) A high-resolution sensor based on tri-aural perception. IEEE Trans on Robotics and Automation, Vol 9, pp 36-48.

[17] Polaroid Corp. (1982) Ultrasonic Range Finders.

[18] Polaroid Corp. (1987) Data sheet for series 7000 transducer. Ultrasonic Components Group, 119 Windsor St., Cambridge, MA.

[19] Politis, Z.; Probert, P.J. (1999), "Target localization and identification using CTFM sonar imaging: the AURBIT Method" Proceedings IEEE International Symposium on Computational Intelligence in Robotics and Automation, 1999. CIRA '99 pp. 256 –261.

[20] Sabatini, A.M. (1997), "A stochastic model of the time of flight noise in airborne sonar ranging systems" IEEE Trans. Ultrasonics, Ferrorelectrics and Freq. Control, Vol 44 No 3, pp. 606-614.

[21] Sabatini, A.M.; Rocchi, A. (1996), "Digital-signal-processing techniques for the design of coded excitation sonar ranging systems" Proceedings IEEE International Conference on Robotics and Automation, pp: 335 –340.

[22] Woodward, P. M. 1964. Probability and Information Theory with Applications to Radar, 2nd edition, Oxford: Pergamon Press.

[23] Yata, T.; Ohya, A.; Yuta, S. 2000, "Use of amplitude of echo for environment recognition by mobile robots", Proceedings IEEE/RSJ Intelligent Robots and Systems, (IROS 2000) Vol 2 , pp. 1298 –1303.